HHS Public Access

Author manuscript

Sci Immunol. Author manuscript; available in PMC 2018 June 08.

Published in final edited form as:

Sci Immunol. 2017 December 08; 2(18): . doi:10.1126/sciimmunol.aao1135.

GPR55 regulates intraepithelial lymphocyte migration dynamics and susceptibility to intestinal damage

Hayakazu Sumida[1], **Erick Lu**[1], **Hsin Chen**[1], **Qiyun Yang**[2], **Ken Mackie**[3], and **Jason G. Cyster**[1,*]

[1]Department of Microbiology and Immunology and Howard Hughes Medical Institute, University of California San Francisco, San Francisco, California 94143, USA

[2]Department of Bioengineering and Therapeutic Sciences, University of California, San Francisco, San Francisco, California 94143, USA

[3]Department of Psychological and Brain Sciences, Gill Center for Biomolecular Science, Indiana University, Bloomington, Indiana 47405, USA

Abstract

Intraepithelial lymphocytes (IELs) of the small intestine are intimately associated with the epithelial cells yet the factors controlling their migration and interaction dynamics are poorly understood. Here we demonstrate that GPR55, a receptor that mediates migration inhibition in response to lysophosphatidylinositol (LPI), negatively regulates TCRγδ IEL accumulation in the small intestine. Intravital imaging studies show GPR55-deficient IELs migrate faster and interact more extensively with epithelial cells. GPR55 also negatively regulates T cell homing to the small intestine and γδT cell egress from Peyer's patches. GPR55-deficiency or short-term antagonist treatment protects from nonsteroidal anti-inflammatory drug-induced increases in intestinal permeability. These findings identify a migration-inhibitory receptor that restrains IEL-epithelial cell crosstalk and show that antagonism of this receptor can protect from intestinal barrier dysfunction.

Introduction

The small intestinal epithelium must achieve a balance between supporting absorption of nutrients while restricting systemic access of gut microbes. A large diversity of intestinal immune cells assist in achieving this balance in humans and mice. The intraepithelial lymphocytes (IELs) are the immune cells most intimately associated with the epithelial cells at a density of about 1 per 10 epithelial cells and they have the most immediate influence on epithelial cell function (1, 2). In humans, IEL numbers increase in several conditions,

*Correspondence to: Jason.Cyster@ucsf.edu.

Author contributions

H.S. and J.G.C designed experiments, interpreted the data and wrote the manuscript. H.S., E.L., and Y.Q. performed experiments and analyzed the data. H.C. analyzed the data. K.M. provided critical materials and helped edit the manuscript.

Competing financial interests

The authors declare no competing financial interests.

including inflammatory bowel disease and celiac disease (2, 3). However, the impact of IEL accumulation on intestinal physiology remains to be fully understood.

In mice, IELs mostly express the CD8αα homodimer and 40–60% are γδT cells (1, 3). Formation of the IEL and lamina propria (LP) lymphocyte compartments is partially dependent on the chemokine receptor CCR9 and its ligand CCL25 (TECK) that is abundantly expressed by small intestine epithelial cells (4, 5). IELs migrate continually within the small intestine between the epithelium and the basement membrane and occasionally move into the lateral intercellular spaces between epithelial cells (6–8). This extensive migratory activity allows for surveillance of the epithelium (9). However, the factors controlling IEL migration dynamics are not fully defined.

In earlier work we found that the orphan G-protein coupled receptor, GPR18, was required for the homeostasis of γδT IELs in the small intestine (5). GPR55 has sequence similarity to GPR18 (10) and we noted that GPR55 was also abundantly expressed in intestinal IELs (ImmGen.org). GPR55 was initially characterized as a cannabinoid-type receptor (11). However, further investigation revealed that lysophosphatidylinositols (LPI) were more potent ligands (12, 13). GPR55 is expressed in a range of cell types beyond IELs, including myeloid cells and neurons (14, 15). *In vitro* and *in vivo* studies have suggested that GPR55 can couple to Gα13 to cause Rho activation and growth cone-repulsive effects (15–17). However, other studies have shown that GPR55 can couple to Gq/11 and that it can have pro-migratory effects (18–22). Therefore, it is possible that the receptor has multiple signaling capabilities and that the G-protein coupling that occurs depends on the cell type. While *in vivo* studies have shown GPR55 regulates the targeting of axons (15), dendrite branching (20), neuropathic pain (23), and bone mass (24), the function of the receptor in immune cells is not understood.

Nonsteroidal anti-inflammatory drugs (NSAIDs), the most widely consumed pharmaceuticals in the world, are a cause of greater than 100,000 hospitalizations per year in the United States due to gastrointestinal (GI) complications (25, 26). In addition to gastric injury, there is an increasing appreciation that many patients suffer damage to the small intestine. Although administering proton pump inhibitors may improve gastric symptoms, there is evidence that they also exacerbate intestinal damage (25) making it important to identify other approaches to protect the small intestine. Deficiency in γδT IELs in mice leads to an increase in the sensitivity of the small intestine to NSAID (indomethacin)-induced injury and to increased pathogen-breaching of the epithelial barrier (9, 27). These findings raise the question of whether increases in IELs can protect from NSAID-induced intestinal injury.

Here we report that GPR55 acts as a migration inhibitory receptor in IELs. GPR55-deficient mice have increased numbers of small intestinal γδT IELs and these cells migrate more extensively in close association with the epithelium. GPR55 also acts as a negative regulator of T cell homing to the small intestine and it antagonizes indomethacin-induced γδT cell egress from Peyer's patches. Importantly, we find that GPR55-deficiency or antagonism protects mice from indomethacin-induced intestinal leakage. Our data suggest that targeting

GPR55 could be a method to augment IEL function in promoting the integrity of the small intestinal epithelium.

Results

GPR55 restrains γδT IEL accumulation in the small intestine

Quantitative PCR analysis on sorted cells revealed GPR55 mRNA was abundantly expressed by all small intestine IELs, with the highest expression being in CD8αα TCRγδ IELs (Fig. 1A). GPR55 was not detected in splenic TCRαβ T cells, was expressed at a low level in splenic TCRγδ T cells, and was minimally expressed by intestinal epithelial cells (Fig. 1A). GPR55 was also detected in intestinal dendritic cells (DCs) and macrophages though at lower levels than in IELs (Fig. 1A). These observations and the lack of understanding about the cues controlling IEL migration dynamics led us to test the impact of GPR55-deficiency on IELs. In mice lacking GPR55, there was a selective increase in IEL γδT cell frequencies and numbers (Fig. 1, B and C). Reciprocally, there was a slight reduction in CD8αβ TCRαβ and CD4 TCRαβ IEL cell frequencies but no change in their number (Fig. 1C). A similar trend was seen for cell frequencies in the LP compartment (Fig. 1C). Spleen and mesenteric lymph node (mLN) T cell frequencies were unaffected (fig. S1A). The procedure we use for IEL isolation involves shaking the intestine in medium (5, 28) and while it isolates IEL at high purity, the yield may be lower than with techniques that employ dithiothreitol (DTT) and/or ethylenediaminetetracetate (EDTA) treatment (29–31). When IELs and lamina propria lymphocytes (LPLs) were isolated with the DTT plus EDTA procedure an increase in their frequency was observed in the GPR55 KO intestine compared to control samples (fig. S1B). This technique yielded more total IEL and led to lower γδT cell representation in the LPL compartment, possibly due to lower contamination by IEL. In summary, we show by two different isolation techniques that GPR55 deficiency leads to increased γδT IELs.

The fraction of γδT IELs expressing Vγ7, the major IEL Vγ, was unaltered by GPR55-deficiency and the cells had similar expression of the maturation marker Thy1, the integrin chains αE (CD103) and β7 (Fig. 1D). Thymic γδT cell frequencies were also not affected by GPR55-deficiency (Fig. 1E). When mice were maintained on BrdU-containing drinking water for 7 days, similar fractions of the control and GPR55 KO IELs became labeled, suggesting that the populations were turning over at similar rates (Fig. 1F). To test whether the role of GPR55 was hematopoietic cell intrinsic, irradiated lymphocyte-deficient (RAG1 KO) mice were reconstituted with GPR55 KO or control bone marrow (BM). Examination after an 8 week reconstitution period showed a prominent over-accumulation of GPR55 KO γδT IELs while other IEL populations were present in numbers equivalent to the controls (Fig. 1G). A similar experiment using a mixed BM transfer confirmed the intrinsic role of GPR55 in IELs (fig. S1C). Vγ7 usage and Thy1 maturation marker expression were again similar between KO and control cells (fig. S1D). Reconstitution of γδ and αβ T cell subsets in the spleen was unaffected by GPR55 deficiency (fig. S1E). In a further experiment, we rescued GPR55 expression in GPR55 KO cells using retroviral gene-transduction of BM cells. In RAG1 KO mice reconstituted with this BM, GPR55 KO γδT IEL were returned towards the normal range whereas splenic T cell populations were not affected by GPR55

transduction (Fig. 1H). These data confirm that the increased IEL frequency in GPR55 KO mice and chimeras was due to loss of GPR55 and not to an off-target effect.

Additional phenotypic analysis revealed comparable expression of the activation markers CD69, CD62L, CD44 and CD25 by GPR55-deficient IELs as well as comparable low expression of IFNγ and IL-17A (fig. S1F). This analysis revealed that GPR55-deficient cells had reduced CCR9 expression in GPR55 KO mice and in mixed BM chimeras (fig. S1G). CCL25 mRNA levels in small intestine tissue did not show a difference between GPR55 KO and control mice (fig. S1G). To rule out the possibility that the difference in IEL frequency in GPR55 KO mice was dependent on altered CCR9 expression we generated GPR55 CCR9 double KO:WT mixed BM chimeras and compared them to CCR9 single KO:WT mixed BM chimeras. GPR55-deficiency led to an over-representation of γδT IELs that was at least as great as that observed on the CCR9-sufficient background (fig. S1H). Taken together, these data establish a cell intrinsic role for GPR55 in restraining IEL accumulation in the small intestine.

GPR55 transmits a migration-inhibitory signal in response to LPI

Previous studies have shown that LPI can function as a ligand for GPR55 in non-lymphoid cells. Using GPR55-overexpressing WEHI231 cells in Transwell migration assays we observed a dose-sensitive migration inhibitory effect of LPI (a mixture of 16:0, 18:0 and 18:2 LPI) on cell migration in response to the WEHI231 cell chemoattractant, CXCL12 (Fig. 2A and fig. S2A). No selective migration inhibitory effect of LPI was observed on control WEHI231 cells transduced with empty vector, even at doses of 10 μM (Fig. 2A). Consistent with GPR55 having a migration inhibitory role, LPI had no pro-migratory effect on GPR55$^+$ WEHI231 cells when tested in the absence of CXCL12 (Fig. 2A). A comparison of different LPI isoforms revealed that the arachidonyl (20:4) form was the most potent inhibitor of GPR55$^+$ cell migration (Fig. 2B).

Studies in non-immune cell types have provided evidence that GPR55 can couple to Gα13 and Gαq/11 (11, 15, 16). We tested whether GPR55-mediated migration inhibition in lymphocytes was dependent on Gα13 using B cells from Gna13$^{f/f}$ Mb1Cre mice that lack Gα13 (32). Lack of Gα13 in GPR55-transduced B lymphocytes resulted in loss of LPI-mediated migration inhibition (Fig. 2C). While these data are not definitive regarding G-protein coupling in IELs, they support the conclusion that Gα13 is required for GPR55-mediated migration inhibition in lymphocytes.

IELs express the chemokine receptor CXCR3 and migrate to its ligand CXCL10 (33) and we used this chemokine in some of our assays because of its robust activity. Although IELs were found to have high baseline motility in Transwell assays, CXCL10-induced augmentation in migration could readily be observed (Fig. 2D). When LPI was combined with CXCL10, IEL migration was dose-dependently inhibited (Fig. 2D). This migration inhibitory effect could be overcome by addition of a GPR55 antagonist, CID16020046 (Fig. 2D). LPI also inhibited IEL migration to the CCR9 ligand, CCL25, and this effect was lost when using cells from GRP55-deficient mice (Fig. 2E). The inhibitory effect of LPI was most potent for γδT IELs, but was also observed with CD8αα and more weakly with CD8αβ TCRαβ IELs (fig. S2B). The CXCL12-induced migration of splenic CD8$^+$ and

CD4$^+$ TCRαβ T cells, whose endogenous GPR55 expression levels are low (Fig. 1A), was unaffected by LPI (fig. S2C).

Signaling via Gα13 causes activation of the small G-protein Rho and this can lead to phosphorylation of the ezrin-radixin-moesin (ERM) proteins by the Rho-effector kinase ROCK (34, 35). Treatment of GPR55 transduced WEHI231 cells with LPI led to an induction of phospho-ERM (pERM) that was not seen in the control cells (Fig. 2F). Exposure of IELs to LPI was sufficient to cause an elevation in pERM in WT CD8αα γδT IELs (Fig. 2F) but not in GPR55 KO CD8αα γδT IELs (Fig. 2F). Taken together, these findings provide evidence that GPR55 signaling in IELs activates a Gα13- and Rho-mediated migration inhibitory pathway.

Recent work demonstrated that LPI is abundant in the colon, cerebellum, liver, lung, spleen, and fat, though levels in the small intestine were not determined (36, 37). Using LC-MS/MS, we detected multiple forms of LPI in the small intestine (Fig. 3A and fig. S3). 18:0 LPI was the most abundant form, but 16:0, 18:1 and 20:4 LPI were all detected in intestinal tissue (Fig. 3A). Notably, the LPI abundance in the small intestine was greater than in spleen. A 20:4 LPI concentration of 1,800 ng/g of tissue, if all the weight of the tissue were assumed to be equally accessible to the lipid, corresponds to a concentration of ~2.8 μM. These data are in accord with the possibility that LPI concentrations in some interstitial microenvironments are in the range that has strong activity on the receptor.

Although LPI is the best-established ligand for GPR55, the receptor has been shown to respond to several other lipid types (14, 15). As a second approach to test for the presence of GPR55 ligands in the intestine we used the migration inhibition technique as a bioassay. Tissue extracts prepared from the small intestine and colon caused GPR55-dependent migration inhibition whereas this effect was not observed with extracts prepared from the spleen (Fig. 3B). Moreover, supernatant from cultured small intestinal epithelial cells were found to generate GPR55 ligand activity using the bioassay (Fig. 3C).

As a further probe for ligand activity in the intestine, we tested the impact of GPR55 over-expression on cell accumulation in the intestine using a BM transduction and irradiated recipient reconstitution approach. Comparing the frequency of control versus GPR55 over-expressing cells in the same animal we observed a striking block in accumulation of GPR55 transduced myeloid cells in the small intestine (Fig. 3, D and E). GPR55 transduction had a more modest impact on the IEL and lamina propria CD8αα γδT cell compartment in the BM chimeras, most likely because the receptor is already very highly expressed in these cells (Fig. 3F). There was no significant effect of GPR55 over-expression on the representation of T cells or myeloid cells in the spleen (Fig. 3G). These findings are in accord with the intestine producing GPR55 ligand(s) that can inhibit the accumulation of GPR55-overexpressing cells in this tissue.

GPR55 limits γδT IEL migration in association with the small intestinal epithelium

To examine IEL distribution in the small intestine, sections from control (GPR55 Het) and GPR55 KO mice were stained with antibodies against the γδTCR (GL3) and CD8α to identify the T cells and against laminin to identify the basement membrane that separates the

epithelium from the LP (Fig. 4A). DAPI (4′,6-diamidino-2-phenylindole) staining of nuclei facilitated identification of the epithelial cell layer. Since the nuclei are situated close to the basolateral side of epithelial cells, the apical surface projects some distance beyond the DAPI signal. Enumeration of CD8αα$^+$ γδTCR$^+$ cells showed that about 28% of the GPR55 Het γδT IELs were situated in close association with epithelial cells, defined as overlapping with or in the space between the fluorescence signal for the epithelial cell nuclei (Fig. 4, A and B, cells highlighted by yellow arrows) while the majority of the IELs were situated in a peri-basement membrane space (PMS) (Fig. 4, A and B, cells highlighted by orange arrows). Importantly, the frequency of GPR55 KO γδT cells in close association with epithelial cells was increased to 35% (Fig. 4B and C).

The impact of GPR55-deficiency on γδT IEL association with epithelial cells was further studied by reconstituting IEL-deficient RAG1 KO mice with an equal mixture of control (GPR55 Het) TCRβ KO and GPR55 KO TCRβ KO TCRδ-eGFP BM (Fig. 4D). The use of TCRβ KO donor mice allowed selective identification of γδT cells using CD8α labeling in the real-time imaging experiments detailed below; the use of RAG1 KO recipients was necessary to avoid contamination of the donor IEL populations by radio-resistant host IELs. When the positioning of control and KO γδT IELs in small intestinal sections was examined using TCRδ-eGFP expression to distinguish mutant and control cells, enrichment for GPR55 KO γδT IELs in association with epithelial cells was again observed (Fig. 4, E and F). In addition, flow cytometric analysis of tissues from these mice revealed a selective over-accumulation of GPR55 KO CD8αα$^+$ γδT IELs in the small intestine relative to their representation in the spleen (Fig. 4G). This over-accumulation was also evident in sections of the small intestine (Fig. 4, E and H). Taken together, these data establish that the influence of GPR55 on cell positioning in close association with epithelial cells is γδT cell intrinsic and they confirm the intrinsic role of the receptor in restraining γδT IEL accumulation in the intestine.

To determine how GPR55 influenced IEL migration dynamics we used real-time 2-photon microscopy. In our first approach, CD8αα IELs were intravitally labeled using anti-CD8α-PE antibody as in our previous work (5). By this approach, we observed an altered CD8α$^+$ IEL migration path in mice lacking GPR55 (Fig. 5A and movies S1 and S2; the CD8α antibody was also bound by some large highly fluorescent cells in the lamina propria). In particular, while GPR55 Het CD8α cells showed transient movements in close association with epithelial cells, GPR55 KO CD8α cells appeared to migrate for longer in a location overlapping with the epithelial cells. Similar findings were made in anti-CD8α-PE antibody treated TCRβ KO mice where only γδT cells were present (fig. S4) or when IEL behavior was examined in TCRδ–eGFP control and GPR55 KO TCRδ–eGFP mice in which the GFP$^+$ cells were tracked (Fig. 5B and movies S3 and S4). To investigate this close association in more detail, we assembled movies from single Z-plane images that most completely captured the TCRδ-eGFP+ cell at each time point (movies S5 and S6). Representative snap shots from GPR55 Het and GPR55 KO movies are shown in Fig. 5C. Movement in close association with the epithelium was observed as overlap with the fluorescence signal of the epithelial cell nuclei (labeled with Hoechst) (Fig. 5C, ovals in right upper panel). Of note, epithelium-probing-like movement, characterized by sharply angled movement into presumed lateral intercellular spaces, were observed similarly in GPR55 Het and KO (Fig.

5C, left two and right lower panels). It should be noted that these movies were taken near the tips of the intestinal villi and in some cases the tips were flattened by the overlying cover glass; the large amount of epithelium immediately above the plane of view may account for the apparent movement of some γδT cells into regions distant from the lateral epithelial cell layers.

To control for variability in the tissue preparation, we adopted a mixed BM chimeric approach to allow side-by-side tracking of control and KO cells. For this analysis we reconstituted RAG1-deficient mice with a mixture of control (GPR55 Het) TCRβ KO and GPR55 KO TCRβ KO TCRδ–eGFP BM (Fig. 4D). The absence of CD8αα and CD8αβ TCRαβ T cells in the mixed BM chimeras ensured that CD8αα γδT cells could be selectively detected using intravital CD8α-PE antibody labeling and that control and KO cells could be distinguished based on eGFP expression (Fig. 5, D and movies S7). Single Z-plane movies (Movie S8) and snap shots (Fig. 5E) showed similar observations to those in TCRδ–eGFP mice. This analysis revealed that GPR55 KO γδT IELs had a higher migration speed than the control γδT cells (Fig. 5F). Comparison of the migratory tracks revealed that the GPR55 KO cells showed a higher percentage of their tracking time in close association with the epithelial cells and a corresponding increase in the duration of each epithelial exploration (Fig. 5 G). There was no difference in the frequency of cells exhibiting lateral intercellular space probing-like movement (Fig. 5H). These data suggest that GPR55 functions to reduce the amount of IEL migration in close association with epithelial cells.

A previous study showed that treatment of mice with anti-CD3 caused upregulation of IFN-inducible genes including *Pkr* and *Usp18* within 3 hrs and this was suggested to reflect direct crosstalk between IELs and epithelial cells (38). In accord with the increased numbers of IELs and their increased overall association with the epithelial cells, anti-CD3 antibody treatment led to a stronger induction of *Pkr* and *Usp18* in the intestine of GPR55 KO mice (Fig. 5I).

GPR55-deficiency protects from indomethacin-induced intestinal permeability

To test the impact of increased IEL association with epithelial cells in a disease setting, NSAID-induced increase in intestinal permeability was examined. This was done by measuring FITC-dextran leakage from the intestine into blood circulation 4 hours after oral indomethacin gavage (27). Indomethacin pretreatment led to a marked (though variable) increase in FITC-dextran levels in the serum of control mice (Fig. 6A). Importantly, GPR55-deficient mice suffered significantly less leakage of FITC-dextran into circulation than matched control mice (Fig. 6A). Oral treatment with the GPR55 antagonist CID16020046 versus carrier for 30 min also reduced the amount of intestinal leakage following indomethacin treatment (Fig. 6B). Reciprocally, IEL-deficient CCR9 KO mice that have a marked reduction in IEL numbers, exhibited increased FITC-dextran leakage after indomethacin treatment (Fig. 6C). Importantly, when mice entirely lacked γδT cells indomethacin-induced intestinal leakage was increased and GPR55-deficiency no longer conferred resistance to leakage (Fig. 6D). These data indicate that GPR55 deficiency in γδT IELs protects mice from indomethacin induced intestinal damage.

One factor that contributes to maintaining intestinal barrier integrity is prostaglandin E2 (PGE2) (26, 39); however, PGE2 was similarly reduced by indomethacin in the intestine of control and GPR55 KO mice (fig. S5). Therefore the reduced leakage in GPR55 KO mice is unlikely to be due to altered PGE2 production.

Immunofluorescence microscopy analysis showed that γδT IEL were further increased above their already elevated numbers in GPR55 KO mice in both the peri-basement membrane space and in close association with epithelial cells following indomethacin treatment (Fig. 6, E and F and fig. S6). The proportion of cells in close association with epithelial cells was not changed by the treatment (Fig. 6G). A smaller increase in IELs was observed in control mice, though this did not reach significance. Flow cytometric analysis of tissue from these mice showed similar findings for the KO mice but did now reveal an increase in the control group (Fig. 6H). The basis for the discrepancy in the controls between the microscopy and flow cytometric analysis is unclear but might reflect differential recovery during tissue digestion or sampling of different regions of the intestine. In summary, indomethacin treatment leads to a rapid increase in γδT IEL numbers in the small intestine and the number of cells continued to be greater in GPR55-deficient than control mice. We suggest that both the greater γδT IEL numbers and their increased association with the epithelium contribute to the protection from indomethacin-induced intestinal damage in the absence of GPR55 function.

GPR55 represses Peyer's patch γδT cell egress and CD8 T cell intestinal homing

The increased total γδT IEL number in the small intestine 4 hours after indomethacin treatment led us to ask whether cells might be rapidly recruited from other site(s). We therefore examined γδT cell distribution and found that indomethacin treatment led to a reproducible drop in CD8αα γδT cells in Peyer's patches (PPs) of KO but not control mice (Fig. 7A). There was also a slight trend for a reduction in CD8αα γδT cells in the mLN at this time point, establishing that the cells lost from PPs were not accumulating in the mLN. CD8αβ TCRαβ cell frequencies in PP, mLN, and blood were unaltered by the indomethacin treatment (fig. S7A). A similar analysis in mixed BM chimeras showed that the KO γδT cells became under represented in the PPs of indomethacin versus control treated mice, establishing that the effect was γδT cell intrinsic (Fig. 7B). Although the selectivity of the PP effect to GPR55 KO mice and the low overall number of γδT cells in this tissue indicated it could not account for all the increase in γδT IELs observed in indomethacin treated mice, we considered it might be a factor involved in the greater γδT IEL increase in KO mice and therefore pursued the mechanism further.

The PP γδT cell loss in indomethacin treated GPR55 KO mice appeared to be due to egress from the PP since it could be prevented by pre-treating with the S1PR1-modulatory and egress-inhibitory drug, FTY720 (Fig. 7C). In Transwell migration assays, PP CD8αα γδT cells, but not other PP αβT cells or B cells, were inhibited in their migration to CXCL12 by LPI in a GPR55-dependent manner (Fig. 7D). Despite these findings indicating that GPR55-deficient cells were emigrating from PPs in an FTY720-sensitive manner, we were unable to detect an increase in CD8αα γδT cell frequency in peripheral blood following indomethacin treatment of GPR55 KO mice or chimeras (Fig. 7, A and B). The explanation

for this is unclear, but it is possible that the emigrating cells spend only very short amounts of time (minutes) in the circulation as has been reported for some other cell types (40, 41). Consistent with cell egress from sites such as PPs contributing to the indomethacin-induced increase in GPR55 KO γδT IELs, FTY720-pretreated control and KO mice no longer showed a significant difference in their accumulation of IELs in the intestine after indomethacin treatment (Fig. 7C).

Finally, we considered whether endogenous GPR55 expression in T cells could limit their access from blood to small intestine as this might be another way in which injury-induced intestinal accumulation of T cells could be negatively regulated by this receptor. Our initial efforts to test this question using adoptive transfers of control and GPR55 KO small intestine-derived IELs were unsuccessful due to the poor recovery of these cells after transfer. In a second approach we asked whether the gut-tropism imprinting factor, retinoic acid, increased GPR55 expression in αβT cells. CD8 T cell activation in the presence of retinoic acid caused upregulation of the intestinal homing receptors CCR9 and α4β7 (Fig. 7E and fig. S7B) as expected (42). Such culture conditions also led to upregulation of *Gpr55* in αβ T cells (Fig. 7E) though not to the level observed on IELs (Fig. 1A). Adoptive transfer of a mixture of WT and GPR55 KO cells from the retinoic acid culture conditions led to a marked enrichment of the KO CD8 T cells in the intestine compared to control cells 1 day after transfer and to a reduction in their representation in spleen and blood (Fig. 7F). By contrast, GPR55 KO CD4 T cells were represented in spleen and blood at a frequency similar to that in the injected cell population (Fig. 7F; the frequency of CD4 T cells in the intestine was too low to quantitate). To confirm that the CD8 T cell homing difference was due to the presence versus absence of GPR55 we repeated the experiment using cells that were cultured in retinoic acid and also transduced with GPR55. GPR55 transduction reversed the IEL accumulation effect observed for GPR55 KO CD8 T cells (Fig. 7G). These findings suggest that GPR55 may function to modulate effector T cell accumulation in the intestine under some conditions.

Discussion

This study identifies GPR55 as a receptor regulating the migratory behavior of intestinal lymphocytes. The receptor acts to restrain the extent of interaction between γδT IEL and intestinal epithelial cells, and it negatively regulates accumulation of cells in the small intestine. We find that LPI, the best-established ligand for GPR55, is abundant in the small intestine and is capable of inhibiting IEL migration. Furthermore, we show that GPR55 deficiency protects from indomethacin-induced intestinal leakage and our data suggest this is a consequence of increased IEL-epithelial cell crosstalk. The activity of a GPR55 antagonist in protecting from indomethacin-induced intestinal leakage may have therapeutic relevance in the context of NSAID-induced and possibly other types of GI disease.

GPR55 has been demonstrated to signal via Gα13 and Gαq/11 heterotrimeric G-proteins (15–22). Our experiments reveal a prominent migration inhibitory action of GPR55 in IEL and PP γδT cells and GPR55 transduced lymphocytes, suggesting that Gα13 may be the prominent form of coupling in these cells. The loss of the migration inhibitory effect of LPI in B lymphocytes lacking Gα13 is consistent with this conclusion though a definitive test

will require Gna13 deletion from CD8αα γδT cells. The ability of LPI to induce ERM phosphorylation is also in accord with Gα13-mediated signaling to Rho and ROCK (43). ERM phosphorylation leads to activation of these cytoskeletal regulatory proteins and has been associated with reduced cell migration (44).

GPR55-deficiency led to an increase in γδT IELs though not in CD8αα TCRαβ or CD8αβ TCRαβ IELs. The selectivity of the population size effect is in accord with γδT cells expressing the highest amounts of GPR55 mRNA and being most strongly inhibited in their migration by LPI. Our cell transfer experiments show that GPR55 can negatively regulate cell migration from the blood to the small intestine and this maybe a contributory factor to the increase in numbers since γδT IELs are maintained in part by influx of precursors from circulation (45). GPR55 may also normally restrain the egress of γδT cells from some tissues, as we reveal for PPs following indomethacin treatment, and this could allow increased availability of cells for homing to the small intestine. Finally, GPR55 might act as a growth regulatory receptor in IELs similarly to the growth regulatory activity of the Gα13-coupled S1PR2 receptor in germinal center B cells (32). Although we did not detect a significant increase in BrdU labeling of γδT IELs, we did note a trend for increased incorporation of this nucleotide, a trend not seen in the other IEL populations in the same mice.

Imaging studies have shown that IELs are highly motile and they frequently move from beneath the epithelial cells to the lateral intercellular space between them (6–8). In accord with their movement being to support surveillance of the epithelium and defense against invaders, a recent study showed rapid movement of IELs into contact with epithelial cells that were being invaded by a bacterial pathogen (9). Moreover, bacterial infection was more severe if the γδT IELs were less able to interact with the epithelial cells due to occludin deficiency. Our work suggests that GPR55 acts to restrain the extent to which IELs move in close association with the epithelial cells. This restraint may be needed to ensure that normal functions of the epithelium are not interfered with. The resolution of our imaging analysis has not allowed us to discern the precise nature of the association between GPR55 KO cells and the epithelium, though it appears to not reflect positioning deep in the lateral intercellular space. Indeed, the frequency with which cells showed the perpendicular movement associated with accessing the lateral intercellular spaces (7–9) was possibly not affected by GPR55-deficiency. We therefore suggest that GPR55 negatively regulates the extent of IEL association with the basolateral parts of the epithelial cells while other cues control probing of the lateral intercellular space. Given the difference in amount of time spent closely associated with the epithelial cells, it will be of interest to determine whether any of the absorptive properties of the epithelium are altered by GPR55 deficiency. It will also be worthwhile to determine whether GPR55, by changing the balance of interaction between immune and epithelial cells, influences properties of the microbiome.

The mechanism of indomethacin-induced damage in the small intestine is not yet well understood but may in part involve direct drug-induced damage of epithelial cells (25, 26). Our studies suggest that GPR55 deficiency increases the resistance to indomethacin-induced intestinal leakage by increasing IEL association with the epithelium. This could be a consequence of both the increase in γδT IELs in the intestine and the increased association

of the cells with the epithelial cells. We favor the latter effect as the most relevant because we saw similar protection from indomethacin after short-term treatment with the GPR55 antagonist, a treatment that did not lead to a significant increase in γδT IEL numbers (unpubl.obs.). Increased densities of γδT cell IELs in association with the epithelium are seen in the human intestine in celiac disease patients (2, 3). While the increase in γδT cell densities correlates with disease severity, it is not yet known whether the γδT IELs have a negative or positive impact on disease symptoms. Our findings raise the possibility that reductions in GPR55 ligand abundance might contribute to the γδT cell accumulation and tight association with the epithelium.

In summary, by identifying a role for GPR55 in regulating immune cell accumulation in the intestine and interaction with the epithelium, our studies point toward a new target for therapeutic manipulation to treat intestinal disease. Moreover, our findings that GPR55 is upregulated in CD8 T cells following activation under conditions of exposure to the gut imprinting factor retinoic acid, the expression of the receptor in some intestinal myeloid cells, and the ability of receptor over-expression to restrain cell homing to the small intestine, lead us to suggest that GPR55 will have additional roles in controlling immune cell accumulation and function in the intestine beyond its actions in IELs.

Materials and Methods

See the Supplementary Materials for Materials and Methods information.

Materials and Methods

Mice and Reagents

C57BL/6J (B6, CD45.2) and congenic B6 CD45.1+ mice were from the Jackson Laboratory, and these strains were intercrossed to generate B6 CD45.1/2 F1 mice. GPR55−/− mice were generated as described (46) and were on a C57BL/6 background. CCR9−/−, Rag1−/−, TCRβ−/−, TCRδ−/− and TCRδ-eGFP (TcrdH2BeGFP) mice were from the Jackson Laboratory. $Gna13^{f/f}$ Mb1Cre mice were as described in (32). To generate BM chimeras, CD45.1+ B6 mice were irradiated by exposure to 1,100 rad of γ–irradiation in two doses 5 h apart and i.v. injected with at least 2×10^6 total BM cells from each genotype of mice as indicated and analyzed after 2–3 months. All chimeras appeared healthy at the time of analysis. Although the input cells were mixed at a 1:1 ratio, the reconstitution efficiencies of the different donor BMs were not always identical, a common occurrence in mixed BM chimera studies. Anti-CD3 (25μg LEAF anti-CD3ε 2C11) was given i.p. and the small intestine (duodenum) harvested for RNA preparation as described (38). Animals were housed in a specific pathogen–free environment in the Laboratory Animal Research Center at the UCSF, and all experiments conformed to ethical principles and guidelines approved by the UCSF Institutional Animal Care and Use Committee.

Indomethacin and FITC-dextran treatment and measurement

Indomethacin (Sigma) treatment was by oral gavage (15 mg/kg in 10% DMSO; control mice were treated with 10% DMSO) and FITC-Dextran (average mol wt 3,000–5,000 from Sigma) was given orally 1 hr later as described (27). FTY720 (Cayman Chemicals)

treatment was with 1mg/kg i.p. injection one day before indomethacin treatment. CID16020046 oral administration [200μl of 25μM in PBS containing 0.25% of dimethyl sulfoxide (DMSO), Sigma] was 30 min before indomethacin administration. Mice were bled and serum prepared with serum separation tubes (BD Microtainer). FITC was detected with a SpectraMax M5 illuminometer (Molecular Devices) and SoftMaxPro Software (Molecular Devices). Instrument settings: Ex 485 nm; Em 538 nm; Cut off 530 nm.

Quantitative RT-PCR

Total RNA from tissues or sorted cells was extracted using an RNeasy kit (Qiagen) and reverse- transcribed. Quantitative PCR was performed as described (47). Data were analyzed using the comparative CT (2-ΔΔCt) method using *Hprt* as the reference. The primers were as follows; Hprt: sense primer, 5′-AGGTTGCAAGCTTGCTGGT-3′ and antisense primer, 5′-TGAAGTACTCATTATAGTCAAGGGCA-3′.

Gpr55: sense primer, 5′-GAGGAACCGCTTTATCTTGGAC-3′ and antisense primer, 5′-GGCAGCAGTTGATGTTGGAGA-3′.

Ccl25: sense primer, 5′-TTTTGCCTGCCTGGTTGC-3′ and antisense primer, 5′-TTGATCCTGTGCTGGTAACCC-3′.

Pkr: sense primer, 5′-GGAGCACGAAGTACAAGCGC-3′ and antisense primer, 5′-GCACCGGGTTTTGTATCGA-3′.

Usp18: sense primer, 5′-TTGGGCTCCTGAGGAAACC-3′ and antisense primer, 5′-CGATGTTGTGTAAACCAACCA-3′.

Ccr9: sense primer, 5′-CCATCACTGTCCTCACTGTCTTC-3′ and antisense primer, 5′-GCAATAGTCTGAGTAACCTGGAAGC-3′.

Cell preparations

Splenocyte, thymocyte, and LN cell suspensions were prepared by mashing the organs through 70-μm cell strainers. IELs and LPLs were isolated as described previously (5). In brief, Peyer's patches were removed, and then the small intestine was opened longitudinally and washed with PBS containing 0.1% BSA, 100 U/ml penicillin, and 100 μg/ml streptomycin three times. The intestines were then shaken with prewarmed DMEM containing penicillin, streptomycin, and 5% FCS for 30 min at 225 rpm, 37°C. Supernatants were separated on a 30–40–80% Percoll density gradient (GE Healthcare), and the cells that layered between the 40–80% fractions were collected as IELs. After IEL isolation, tissues were shaken in RPMI 1640 containing 5 mM EDTA and 5% FCS at 175 rpm, 37°C for 15 min. This step was repeated four times and the supernatants were discarded. LPLs were then isolated after digestion in RPMI-1640 supplemented with 0.5 mg/ml collagenase type II (Worthington Biochemical Corporation), 0.1 mg/ml DNase I (Sigma-Aldrich), and 10% FCS at 200 rpm, 37°C for 30 min. In some experiments (fig. S1B), IELs were isolated by shaking (at 225 rpm) with $Ca2^{+}$- and $Mg2^{+}$-free HBSS containing 5% FCS, 1mM DTT, and 5mM EDTA at 37°C for 30 min, and then after discarding medium from further two-time incubation, LPLs were isolated by digestion in RPMI-1640 with 0.5 mg/ml collagenase type

II, 0.1 mg/ml DNase I, and 10% FCS at 200 rpm, 37°C for 30 min. Released cells were then subjected to Percoll fractionation as described above for isolation of IELs. In some cases, epithelial cells were isolated from the 30% Percoll layer and cultured o/n in cell migration medium (RPMI+0.1% fatty acid free BSA+P/S+10mMHEPES+Q(Glu)+βME).

Antibodies and flow cytometry

Cells were stained using standard procedures for surface markers. The following monoclonal antibodies were used for flow cytometry: TCRγδ (GL3; BD or BioLegend), TCRβ (H57; BioLegend), CD3ε (145-2C11; TONBO bioscience), CD4 (GK1.5; BioLegend), CD8α (53.6.7; Tonbo Bio), CD8β (H35; eBioscience), β7 integrin (M293; BD), Thy1.1 (OX-7; BioLegend), Thy1.2 (30-H12; BD), CD19 (6D5; BioLegend), EpCAM (G8.8; BioLegend), CD11b (M1/70; TONBO bioscience), CD11c (N418; TONBO bioscience), F4/80 (BM8.1; TONBO bioscience), MHCII I-A/I-E (M5/114.15.2; eBioscience), MHCII I-Ab (AF6-120.1; BioLegend), B220 (RA3-6B2; TONBO bioscience), CD45.1 (A20; BioLegend), CD45.2 (104; BioLegend), CD69 (H1.2F3; BioLegend), CD62L (MEL-14; BioLegend), CD44 (IM7; BD), CD25 (PC61; BioLegend), IFNγ (XMG1.2; BD), and IL-17A (eBio17B7; eBioscience). Vγ7 antibody was provided by P. Pereira (Institut Pasteur, Paris, France). Dead cells were excluded using Fixable Viability Dye eFluor780 (eBioscience). For FACS sorting, subpopulations of gut CD45+ CD3ε+ T cells were gated as follows: CD8αα TCRγδ, CD8α+CD8β−GL3+TCRβ−; CD8αα TCRαβ, CD8α+CD8β−GL3−TCRβ+; CD8 αβ TCR αβ, CD8α+CD8β+GL3−TCRβ+; CD4 TCRαβ, CD4+TCRβ+. IELs were more than 95% pure. Epithelial cells were isolated as CD45− EpCAM+ viable cells at 80–90% purity. Small intestine lamina propria CD103+CD11b+ dendritic cells and CD103−CD11b+ macrophages were pregated on CD3ε−B220−CD11c+MHCII+ and then isolated as CD103+CD11b+ and CD103−CD11b+F4/80+ at 90% purity, respectively. For BrdU incorporation analysis, mice were given water containing 0.5 mg/ml BrdU for 7 d. Staining was performed with a BrdU flow kit (BD) according to the manufacturer's instructions. For pERM staining, cells were starved for 30min and then treated with LPI for 5 min and then fixed at a final concentration of 1.5% PFA for 10 min at room temperature (21–23°C) and then permeabilized in ice-cold methanol. Cells were washed twice in staining buffer, blocked with Fc-block (2.4G2; BioXcell) and 5% normal goat serum for 20 min at room temperature, stained for 45 min at room temperature for phosphorylated ERM (antibody name; Cell Signaling Technology) followed by goat antibody to rabbit IgG conjugated to Alexa Fluor 647 (A21245; Invitrogen) and in the case of IEL, with appropriate surface markers. For intracellular staining, harvested IELs were stimulated with 100 ng/ml phorbol myristate acetate (PMA) and 1μg/ml ionomycin for 4–5 hours in the presence of GolgiPlug (Brefeldin A, BD). After culture, cells were stained for surface markers then fixed and permeabilized with Cytofix/Cytoperm (BD) and stained for intracellular cytokines. Flow cytometric analysis was performed using a BD LSRII. Sorting was with a BD Aria instrument.

Cell transfers, migration assays and bioassays

For transfers of T cells activated under conditions promoting gut tropism, T cells from LNs of each genotype were stimulated with plate-bound CD3 and CD28 plus 100 ng/ml retinoic acid (Sigma) for 3 d and then resuspended in complete RPMI1640 media with 100 U/ml

IL-2 plus 100 ng/ml retinoic acid. At day 5, cells were harvested and transferred into WT recipients. In some cases cells were transduced with GPR55 or control retrovirus at day 2 and 3 of culture. Transwell migration assays were with 5-μm transwells and were performed as described previously (Ngo et al., 1998) using 10^6 IELs prepared by the Percoll density gradient method above or with the indicated cell types. Sigma LPI (Cat # 62966) contained a mixture of C16:0 (58%), C18:0 and C18:2 (42%) forms of LPI. Avanti LPI was either 16:0, 18:0, 18:1, or 20:4 (*sn*-1). CCL25 was from MyBioSource, CXCL10 and CXCL12 were from PeproTech. The bioassay for GPR55 ligand activity was performed as described (48) with modifications. GPR55 transduced WEHI231 cells were used and the tissue extract was mixed with CXCL12 (100ng/ml) as indicated.

Immunofluorescence

Cryosections of 7 μm were fixed and stained as previously described (5) after fixation with 4% PFA. Staining was with the following antibodies: Laminin (Invitrogen), CD8α (53.6.7; Tonbo Bio), TCRγδ (GL3; BD or BioLegend), and DAPI (Invitrogen). Images were all acquired with AxioVision using an Axio Observer Z1 microscope (Carl Zeiss).

Intravital two-photon microscopy

Control and GPR55 KO mice on a non-transgenic, TCRδ-eGFP transgenic and/or TCRβ KO background, and mixed BM chimeras, were i.v. injected with 10 μg anti–CD8α-PE (BioLegend) 4 h before imaging. After anesthetization, mice were injected i.v. with Hoechst 33342 dye (Invitrogen), and the middle region of the small intestine (jejunum or proximal ileum) was exposed and opened along the anti-mesenteric border with cauterizer tool (Bovie high temp cautery pen, fine tip, ref AA01, Moore Medical) to expose the mucosal side. The tissue was immobilized on thermal dough using 3M Vetbond Adhesive (World Precision). Then, a ring with coverslip and metal pins was put on the mucosal side to stabilize the observation field (8). Images were acquired with ZEN2012 (Carl Zeiss) using a 7MP two-photon microscope (Carl Zeiss) equipped with a Chameleon laser (Coherent). Excitation wavelength was 890 nm. Images were acquired by taking 9–12-μm Z-stacks at 3-μm steps every 20 s. Each XY plane spans 512 × 512 pixels. Videos were made and analyzed with Imaris 7.4 ×64 (Bitplane). Due to difficulties in automatic tracking from the high background of CD8αPE and eGFP signals and overlapping paths, manual tracking was performed. Images for single Z-plane movies were selected using MetaMorph software (ver. 7.7.0.0; Molecular Devices), with the Z-plane chosen at each time point as the one that captured most clearly the IEL being tracked, and then movies were generated with Imaris software.

Retroviral transduction

Cells (WT or GPR55−/−) were retrovirally transduced (32) with MSCV2.2 retroviral vectors containing GPR55 or empty vector and an IRES–Thy1.1 reporter. Virus was produced using PatE cells grown in DMEM+10%FCS+P/S+10mMHEPES+Q(Glu) (without P/S during transfection). For B cells ($Gna13^{f/f}$ Mb1Cre) WT splenic B cells were activated with 0.25 mg/ml anti-CD180 (RP-105; clone RP14, BD Biosciences) and cultured for 24 h. The activated B cells were spin-infected for 2 h with retroviral supernatant, and cultured overnight before use in migration assays. T cells were transduced at day 2 and 3 of culture

with anti-CD3, anti-CD28, IL-2 and retinoic acid as described above. BM cells were harvested 4 days after 5-flurouracil (Sigma) injection and cultured in the presence of recombinant IL-3, IL-6, and mouse stem cell factor (SCF) (100ng/ml, Peprotech). BM cells were spin-infected twice with a retroviral construct expressing GPR55 and an IRES–Thy1.1 cassette as a reporter. One day after the last spin infection, cells were injected into lethally irradiated C57BL/6 recipients.

LC/MS/MS analysis

Samples of snap frozen tissue were placed into homogenization tubes containing 7 homogenizer beads and 10 volumes of ddH2O was added. For example, 150μL ddH2O was added to 15mg of tissue. Tissue samples were homogenized using a Precellys 24 homogenizer with a Cryolys cooling unit (Bertin Technologies). Samples were homogenized using cycle #1 (3 cycles, 20 seconds each, 5000rpm, with 30 second breaks). After homogenization, 20μL of sample was transferred to a 1.5ml eppendorf tube. 20μL of water and 20μL of internal standard solution (100ng/mL stock of 17:1 LPI) was added and the tube was vortexed. 100μL of methanol was then added and the tube was vortexed and then centrifuged at 3000rpm for 10 min in a cooled centrifuge. The supernatant was transferred to a new tube and centrifuged again as before. The resulting supernatant was transferred to a HPLC tube. Samples (10μl volume) were injected into a Shimadzu Nexera X2 HPLC equipped with LC-30AD pumps and a SIL-30AC autosampler. Separation was achieved on a phenomenex Prodigy ODS3 column (150 × 4.6 mm, 5 micron, 00F-4097-E0) using an isocratic flow of mobile phase consisting of 24% mobile phase A (100% H_2O) and 74% mobile phase B (ACN/H_2O [70%/30%, vol/vol] containing 0.7 mM ammonium formate [NH_4HCO_2]) for 7.5 minutes at a total flow rate of 1mL/min. Mass spectrometric detection was performed using an AB SCIEX QTRAP 6500 mass spectrometer. LPI species were detected using multiple reaction monitoring (MRM) in negative ion mode using the transitions (m/z) 571.3→255, 599.2→ 283, 597.2→281, and 619.2→303, and 583.2→267.1 for 16:0 LPI, 18:0 LPI, 18:1 LPI, 20:4 LPI, and 17:1 LPI (internal standard), respectively. The ion source temperature was maintained at 660°C. Curtain gas (CUR), collision gas (CAD), gas 1 (GS1), and gas 2 (GS2) were set at 20, −3, 60, and 60, respectively. The entrance potential (EP) was set at −10 V. The declustering potential (DP) and collision cell exit potential (CXP) were −50 V and −10 V, respectively. Collision energy (CE) was −35 eV for all compounds. Standard curves were generated using LPI reference standards purchased from Avanti Polar Lipids. Quantitation was performed based on the peak area ratio. Data acquisition and quantitative processing were accomplished using the Applied Biosystems Analyst version 1.6.2 software. For PGE_2 analysis, PGE_2 (mrm: 351.2→271; Cayman Chemicals; 363-24-6) was used to generate a standard curve and PGE_2-d4 (mrm: 355.2→275; 34210-10-1) was used as an internal standard. The same column and an isocratic flow of 47% mobile phase A and 53% mobile phase B for 4.2 minutes at a flow rate of 1mL/min was used.

Statistical analysis

Prism (GraphPad, ver. 5.0a) software was used for all statistical analyses. Two-tailed, unpaired Student's *t*-tests or paired *t*-tests were performed when comparing only two groups, and one-way analysis of variance (ANOVA) using Bonferroni's post hoc test for the

indicated comparisons was performed when comparing one variable across multiple groups. *P* values less than 0.05 were considered significant. In graphs, horizontal lines indicate means, and error bars indicate standard error of the mean (SEM).

Supplementary Material

Refer to Web version on PubMed Central for supplementary material.

Acknowledgments

We thank D. Mucida and B. Sgarbi Reis for advise regarding IEL 2P microscopy, P. Pereira for the Vγ7 antibody, L. Hooper for advise regarding indomethacin treatment, C. Lowell for us of the illuminometer, L. Lanier and A. Ma for RAG1−/− mice, T. Roth for help with imaging analysis methods, and Jinping An and Ying Xu for expert technical assistance.

Funding

H.S. was supported by a Japanese Society for Promotion of Science (JSPS) Overseas Research Fellowship, Uehara Memorial Foundation Research Fellowship, The Cell Science Research Foundation, and Mochida Memorial Foundation for Memorial and Pharmaceutical Research, E.L. by a NSF graduate fellowship, H.C. by a CRI Irvington postdoctoral fellowship. J.G.C is an investigator of the Howard Hughes Medical Institute. This work was supported in part by NIH grant AI045073 and DA021696.

References and Notes

1. Hayday A, Theodoridis E, Ramsburg E, Shires J. Intraepithelial lymphocytes: exploring the Third Way in immunology. Nat Immunol. 2001; 2:997–1003. [PubMed: 11685222]
2. Abadie V, Discepolo V, Jabri B. Intraepithelial lymphocytes in celiac disease immunopathology. Seminars in immunopathology. 2012; 34:551–566. [PubMed: 22660791]
3. Cheroutre H, Lambolez F, Mucida D. The light and dark sides of intestinal intraepithelial lymphocytes. Nat Rev Immunol. 2011; 11:445–456. [PubMed: 21681197]
4. Kunkel EJ, Campbell DJ, Butcher EC. Chemokines in lymphocyte trafficking and intestinal immunity. Microcirculation. 2003; 10:313–323. [PubMed: 12851648]
5. Wang X, Sumida H, Cyster JG. GPR18 is required for a normal CD8alphaalpha intestinal intraepithelial lymphocyte compartment. J Exp Med. 2014; 211:2351–2359. [PubMed: 25348153]
6. Chennupati V, Worbs T, Liu X, Malinarich FH, Schmitz S, Haas JD, Malissen B, Forster R, Prinz I. Intra- and intercompartmental movement of gammadelta T cells: intestinal intraepithelial and peripheral gammadelta T cells represent exclusive nonoverlapping populations with distinct migration characteristics. J Immunol. 2010; 185:5160–5168. [PubMed: 20870939]
7. Edelblum KL, Shen L, Weber CR, Marchiando AM, Clay BS, Wang Y, Prinz I, Malissen B, Sperling AI, Turner JR. Dynamic migration of gammadelta intraepithelial lymphocytes requires occludin. Proc Natl Acad Sci U S A. 2012; 109:7097–7102. [PubMed: 22511722]
8. Sujino T, London M, Hoytema van Konijnenburg DP, Rendon T, Buch T, Silva HM, Lafaille JJ, Reis BS, Mucida D. Tissue adaptation of regulatory and intraepithelial CD4(+) T cells controls gut inflammation. Science. 2016; 352:1581–1586. [PubMed: 27256884]
9. Edelblum KL, Singh G, Odenwald MA, Lingaraju A, El Bissati K, McLeod R, Sperling AI, Turner JR. gammadelta Intraepithelial Lymphocyte Migration Limits Transepithelial Pathogen Invasion and Systemic Disease in Mice. Gastroenterology. 2015; 148:1417–1426. [PubMed: 25747597]
10. Ashton JC. Phylogenetic methods in drug discovery. Curr Drug Discov Technol. 2013; 10:255–262. [PubMed: 23895575]
11. Ryberg E, Larsson N, Sjogren S, Hjorth S, Hermansson NO, Leonova J, Elebring T, Nilsson K, Drmota T, Greasley PJ. The orphan receptor GPR55 is a novel cannabinoid receptor. Br J Pharmacol. 2007; 152:1092–1101. [PubMed: 17876302]

12. Oka S, Toshida T, Maruyama K, Nakajima K, Yamashita A, Sugiura T. 2-Arachidonoyl-sn-glycero-3-phosphoinositol: a possible natural ligand for GPR55. J Biochem. 2009; 145:13–20. [PubMed: 18845565]
13. Yin H, Chu A, Li W, Wang B, Shelton F, Otero F, Nguyen DG, Caldwell JS, Chen YA. Lipid G protein-coupled receptor ligand identification using beta-arrestin PathHunter assay. J Biol Chem. 2009; 284:12328–12338. [PubMed: 19286662]
14. Henstridge CM, Balenga NA, Kargl J, Andradas C, Brown AJ, Irving A, Sanchez C, Waldhoer M. Minireview: recent developments in the physiology and pathology of the lysophosphatidylinositol-sensitive receptor GPR55. Mol Endocrinol. 2011; 25:1835–1848. [PubMed: 21964594]
15. Guy AT, Nagatsuka Y, Ooashi N, Inoue M, Nakata A, Greimel P, Inoue A, Nabetani T, Murayama A, Ohta K, Ito Y, Aoki J, Hirabayashi Y, Kamiguchi H. NEURONAL DEVELOPMENT. Glycerophospholipid regulation of modality-specific sensory axon guidance in the spinal cord. Science. 2015; 349:974–977. [PubMed: 26315437]
16. Henstridge CM, Balenga NA, Ford LA, Ross RA, Waldhoer M, Irving AJ. The GPR55 ligand L-alpha-lysophosphatidylinositol promotes RhoA-dependent Ca2+ signaling and NFAT activation. FASEB J. 2009; 23:183–193. [PubMed: 18757503]
17. Obara Y, Ueno S, Yanagihata Y, Nakahata N. Lysophosphatidylinositol causes neurite retraction via GPR55, G13 and RhoA in PC12 cells. PLoS One. 2011; 6:e24284. [PubMed: 21904624]
18. Ford LA, Roelofs AJ, Anavi-Goffer S, Mowat L, Simpson DG, Irving AJ, Rogers MJ, Rajnicek AM, Ross RA. A role for L-alpha-lysophosphatidylinositol and GPR55 in the modulation of migration, orientation and polarization of human breast cancer cells. Br J Pharmacol. 2010; 160:762–771. [PubMed: 20590578]
19. Hofmann NA, Yang J, Trauger SA, Nakayama H, Huang L, Strunk D, Moses MA, Klagsbrun M, Bischoff J, Graier WF. The GPR 55 agonist, L-alpha-lysophosphatidylinositol, mediates ovarian carcinoma cell-induced angiogenesis. Br J Pharmacol. 2015; 172:4107–4118. [PubMed: 25989290]
20. Cherif H, Argaw A, Cecyre B, Bouchard A, Gagnon J, Javadi P, Desgent S, Mackie K, Bouchard JF. Role of GPR55 during Axon Growth and Target Innervation. eNeuro. 2015; 2
21. Andradas C, Blasco-Benito S, Castillo-Lluva S, Dillenburg-Pilla P, Diez-Alarcia R, Juanes-Garcia A, Garcia-Taboada E, Hernando-Llorente R, Soriano J, Hamann S, Wenners A, Alkatout I, Klapper W, Rocken C, Bauer M, Arnold N, Quintanilla M, Megias D, Vicente-Manzanares M, Uriguen L, Gutkind JS, Guzman M, Perez-Gomez E, Sanchez C. Activation of the orphan receptor GPR55 by lysophosphatidylinositol promotes metastasis in triple-negative breast cancer. Oncotarget. 2016; 7:47565–47575. [PubMed: 27340777]
22. Kargl J, Andersen L, Hasenohrl C, Feuersinger D, Stancic A, Fauland A, Magnes C, El-Heliebi A, Lax S, Uranitsch S, Haybaeck J, Heinemann A, Schicho R. GPR55 promotes migration and adhesion of colon cancer cells indicating a role in metastasis. Br J Pharmacol. 2016; 173:142–154. [PubMed: 26436760]
23. Staton PC, Hatcher JP, Walker DJ, Morrison AD, Shapland EM, Hughes JP, Chong E, Mander PK, Green PJ, Billinton A, Fulleylove M, Lancaster HC, Smith JC, Bailey LT, Wise A, Brown AJ, Richardson JC, Chessell IP. The putative cannabinoid receptor GPR55 plays a role in mechanical hyperalgesia associated with inflammatory and neuropathic pain. Pain. 2008; 139:225–236. [PubMed: 18502582]
24. Whyte LS, Ryberg E, Sims NA, Ridge SA, Mackie K, Greasley PJ, Ross RA, Rogers MJ. The putative cannabinoid receptor GPR55 affects osteoclast function in vitro and bone mass in vivo. Proc Natl Acad Sci U S A. 2009; 106:16511–16516. [PubMed: 19805329]
25. Wallace JL. NSAID gastropathy and enteropathy: distinct pathogenesis likely necessitates distinct prevention strategies. Br J Pharmacol. 2012; 165:67–74. [PubMed: 21627632]
26. Boelsterli UA, Redinbo MR, Saitta KS. Multiple NSAID-induced hits injure the small intestine: underlying mechanisms and novel strategies. Toxicol Sci. 2013; 131:654–667. [PubMed: 23091168]
27. Ismail AS, Severson KM, Vaishnava S, Behrendt CL, Yu X, Benjamin JL, Ruhn KA, Hou B, DeFranco AL, Yarovinsky F, Hooper LV. Gammadelta intraepithelial lymphocytes are essential mediators of host-microbial homeostasis at the intestinal mucosal surface. Proc Natl Acad Sci U S A. 2011; 108:8743–8748. [PubMed: 21555560]

28. Jiang W, Wang X, Zeng B, Liu L, Tardivel A, Wei H, Han J, MacDonald HR, Tschopp J, Tian Z, Zhou R. Recognition of gut microbiota by NOD2 is essential for the homeostasis of intestinal intraepithelial lymphocytes. J Exp Med. 2013; 210:2465–2476. [PubMed: 24062413]
29. Mucida D, Park Y, Kim G, Turovskaya O, Scott I, Kronenberg M, Cheroutre H. Reciprocal TH17 and regulatory T cell differentiation mediated by retinoic acid. Science. 2007; 317:256–260. [PubMed: 17569825]
30. Welty NE, Staley C, Ghilardi N, Sadowsky MJ, Igyarto BZ, Kaplan DH. Intestinal lamina propria dendritic cells maintain T cell homeostasis but do not affect commensalism. J Exp Med. 2013; 210:2011–2024. [PubMed: 24019552]
31. Weigmann B, Tubbe I, Seidel D, Nicolaev A, Becker C, Neurath MF. Isolation and subsequent analysis of murine lamina propria mononuclear cells from colonic tissue. Nat Protoc. 2007; 2:2307–2311. [PubMed: 17947970]
32. Muppidi JR, Schmitz R, Green JA, Xiao W, Larsen AB, Braun SE, An J, Xu Y, Rosenwald A, Ott G, Gascoyne RD, Rimsza LM, Campo E, Jaffe ES, Delabie J, Smeland EB, Braziel RM, Tubbs RR, Cook JR, Weisenburger DD, Chan WC, Vaidehi N, Staudt LM, Cyster JG. Loss of signalling via Galpha13 in germinal centre B-cell-derived lymphoma. Nature. 2014; 516:254–258. [PubMed: 25274307]
33. Dwinell MB, Lugering N, Eckmann L, Kagnoff MF. Regulated production of interferon-inducible T-cell chemoattractants by human intestinal epithelial cells. Gastroenterology. 2001; 120:49–59. [PubMed: 11208713]
34. Matsui T, Maeda M, Doi Y, Yonemura S, Amano M, Kaibuchi K, Tsukita S, Tsukita S. Rho-kinase phosphorylates COOH-terminal threonines of ezrin/radixin/moesin (ERM) proteins and regulates their head-to-tail association. J Cell Biol. 1998; 140:647–657. [PubMed: 9456324]
35. Worzfeld T, Wettschureck N, Offermanns S. G(12)/G(13)-mediated signalling in mammalian physiology and disease. Trends Pharmacol Sci. 2008; 29:582–589. [PubMed: 18814923]
36. Masquelier J, Muccioli GG. Development and validation of a specific and sensitive HPLC-ESI-MS method for quantification of lysophosphatidylinositols and evaluation of their levels in mice tissues. J Pharm Biomed Anal. 2016; 126:132–140. [PubMed: 27208623]
37. Okudaira M, Inoue A, Shuto A, Nakanaga K, Kano K, Makide K, Saigusa D, Tomioka Y, Aoki J. Separation and quantification of 2-acyl-1-lysophospholipids and 1-acyl-2-lysophospholipids in biological samples by LC-MS/MS. J Lipid Res. 2014; 55:2178–2192. [PubMed: 25114169]
38. Swamy M, Abeler-Dorner L, Chettle J, Mahlakoiv T, Goubau D, Chakravarty P, Ramsay G, Reis e Sousa C, Staeheli P, Blacklaws BA, Heeney JL, Hayday AC. Intestinal intraepithelial lymphocyte activation promotes innate antiviral resistance. Nature communications. 2015; 6:7090.
39. Sigthorsson G, Simpson RJ, Walley M, Anthony A, Foster R, Hotz-Behoftsitz C, Palizban A, Pombo J, Watts J, Morham SG, Bjarnason I. COX-1 and 2, intestinal integrity, and pathogenesis of nonsteroidal anti-inflammatory drug enteropathy in mice. Gastroenterology. 2002; 122:1913–1923. [PubMed: 12055598]
40. Wright DE, Wagers AJ, Gulati AP, Johnson FL, Weissman IL. Physiological migration of hematopoietic stem and progenitor cells. Science. 2001; 294:1933–1936. [PubMed: 11729320]
41. Liu K, Waskow C, Liu X, Yao K, Hoh J, Nussenzweig M. Origin of dendritic cells in peripheral lymphoid organs of mice. Nat Immunol. 2007; 8:578–583. [PubMed: 17450143]
42. Edele F, Molenaar R, Gutle D, Dudda JC, Jakob T, Homey B, Mebius R, Hornef M, Martin SF. Cutting edge: instructive role of peripheral tissue cells in the imprinting of T cell homing receptor patterns. J Immunol. 2008; 181:3745–3749. [PubMed: 18768825]
43. Siehler S. Regulation of RhoGEF proteins by G12/13-coupled receptors. Br J Pharmacol. 2009; 158:41–49. [PubMed: 19226283]
44. Parameswaran N, Gupta N. Re-defining ERM function in lymphocyte activation and migration. Immunol Rev. 2013; 256:63–79. [PubMed: 24117813]
45. Guy-Grand D, Vassalli P, Eberl G, Pereira P, Burlen-Defranoux O, Lemaitre F, Di Santo JP, Freitas AA, Cumano A, Bandeira A. Origin, trafficking, and intraepithelial fate of gut-tropic T cells. J Exp Med. 2013; 210:1839–1854. [PubMed: 23918956]
46. Wu CS, Zhu J, Wager-Miller J, Wang S, O'Leary D, Monory K, Lutz B, Mackie K, Lu HC. Requirement of cannabinoid CB(1) receptors in cortical pyramidal neurons for appropriate

development of corticothalamic and thalamocortical projections. Eur J Neurosci. 2010; 32:693–706. [PubMed: 21050275]

47. Yi T, Wang X, Kelly LM, An J, Xu Y, Sailer AW, Gustafsson JA, Russell DW, Cyster JG. Oxysterol gradient generation by lymphoid stromal cells guides activated B cell movement during humoral responses. Immunity. 2012; 37:535–548. [PubMed: 22999953]
48. Lu E, Dang EV, Cyster JG. Distinct oxysterol requirements for positioning naive and activated dendritic cells in the spleen. Science Immunology. 2017; 2:eaal5237. [PubMed: 28738017]

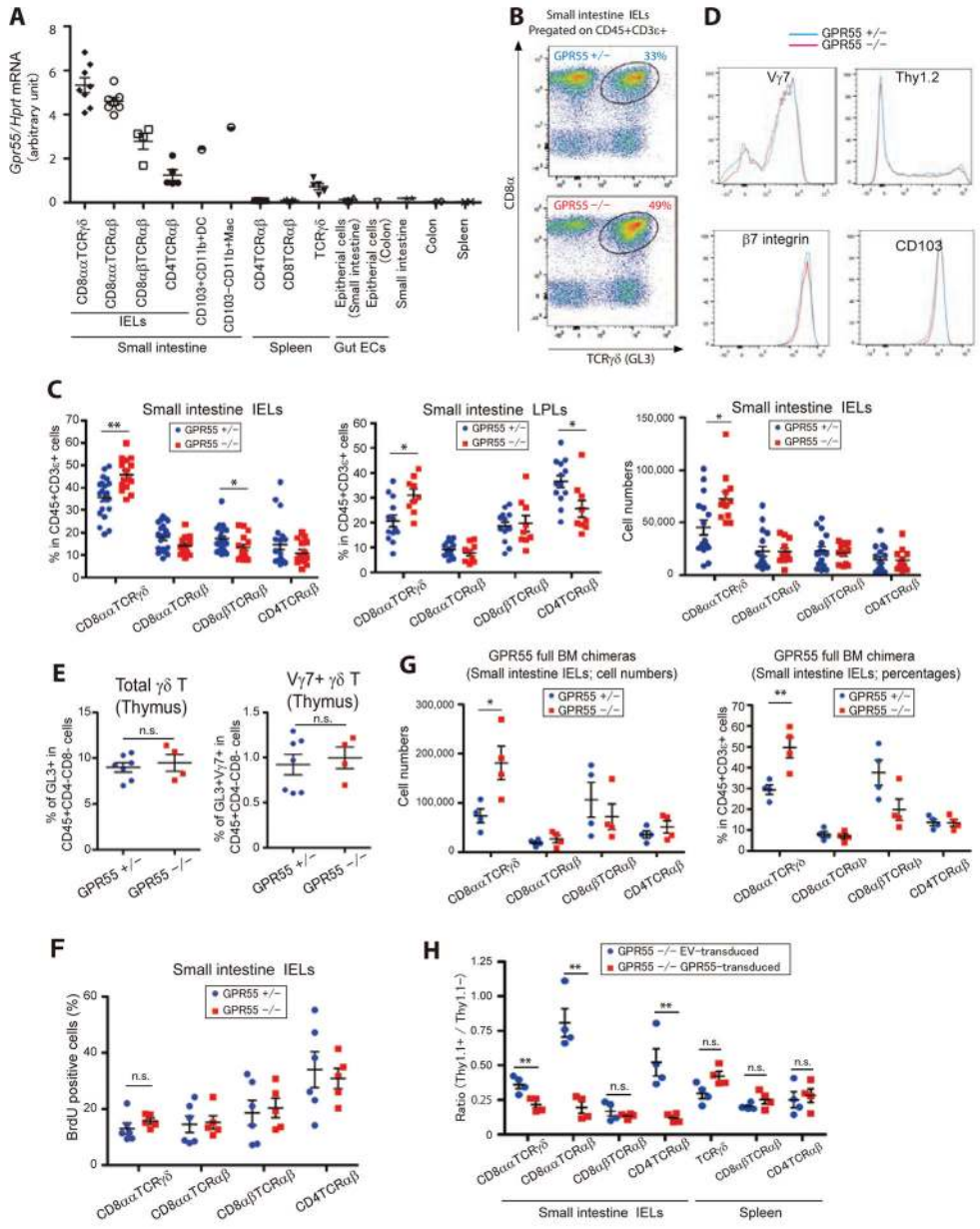

Fig. 1. GPR55 restrains IEL accumulation in the small intestine

(**A**) *Gpr55* transcript abundance in the indicated cell subsets relative to *Hprt*. Each point indicates cells sorted from an individual mouse (except for intestinal DCs and macrophages that were sorted from pooled samples of 10 mice) and lines indicate mean ± SEM. (**B**) Flow cytometric analysis of CD8α and TCRγδ expression by small intestinal IELs from the indicated mice. Number shows fraction of cells in the indicated gate. (**C**) Frequency of intraepithelial lymphocytes (IELs) and lamina propria lymphocytes (LPLs) (left and center panels) and number of IELs (right panel) in the indicated mice. Each population was pre-gated on $CD45^{+}CD3\varepsilon^{+}$ cells. Each point represents data from an individual mouse and lines represent means ± SEM. Left panel: GPR55 Het, *n*=20; GPR55 KO, *n*=15. Center panel: GPR55 Het, *n*=13; GPR55 KO, *n*=9. Right panel: GPR55 Het, *n*=16; GPR55 KO, *n*=12. (**D**)

Expression of Vγ7, Thy1.2, β7 integrin and CD103 (αE integrin) on CD8α+CD8β− GL3+ IELs from GPR55 Het and KO mice. (**E**) Percentage of GL3+ cells among the CD4 and CD8 double negative thymocyte population (left panel) and the fraction of these cells that express Vγ7 (right panel). GPR55 Het, n=7; GPR55 KO, n=4. (**F**) Frequency of IELs of the indicated types that had incorporated BrdU after a 1 week labeling period. GPR55 Het, n=6; GPR55 KO, n=5. (**G**) Number (left) and frequency (right) of IELs of the indicated types in irradiated WT mice reconstituted with GPR55 Het or KO BM. GPR55 Het, n=4; GPR55 KO, n=4. Data are representative of two independent experiments. **(H)** Ratio of GPR55 or empty vector (EV) transduced cells compared to untransduced cells of the indicated types in BM chimeras reconstituted with GPR55 KO BM transduced with the indicated retroviral constructs. Thy1.1 marks transduced cells. $^{**}p<0.01$, $^{*}p<0.05$, 'n.s.' $p>0.05$ by Student's t-test.

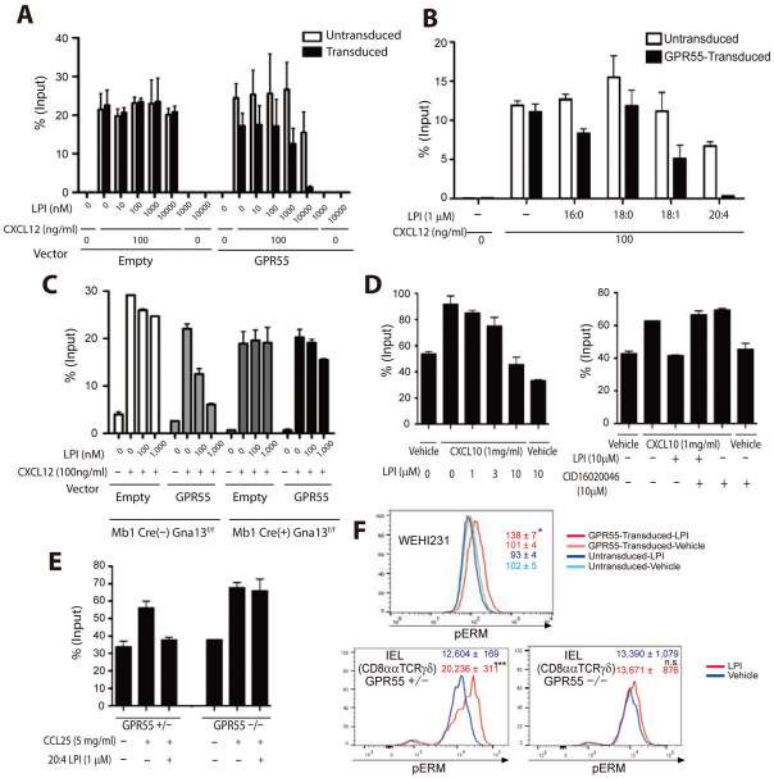

Fig. 2. GPR55 mediates lymphocyte migration inhibition via Gα13

(**A**, **B**) Migration of GPR55 and control transduced WEHI231 cells to CXCL12 and the indicated amounts of LPI (mixture of 16:0, 18:0 and 18:2) (**A**) or 1μM of the indicated types of LPI (**B**) in Transwell assays. (**C**) Migration of empty vector or GPR55-transduced B cells that either express (Mb1Cre− Gna13$^{f/f}$) or lack (Mb1Cre+ Gna13$^{f/f}$) Gα13 to CXCL12 and the indicated amounts of 20:4 LPI. (**D**) Migration of γδT IELs to vehicle or CXCL10 and the indicated amounts of LPI (16:0, 18:0 and 18:2) or the GPR55 antagonist CID16020046. (**E**) Migration of control (Het) or GPR55 KO γδT IELs to vehicle or CCL25 in the absence or presence of 20:4 LPI. (**F**) Flow cytometric analysis of phospho-ezrin-radixin-moesin (pERM) levels in WEHI231 cells (upper panel) or CD8αα γδT IELs from control (Het) or GPR55 KO mice (lower panels) after treatment for 5 min with vehicle (DMSO) or 20:4 LPI (1μM). Each experiment was performed in duplicate and repeated at least twice. Numbers inside plots indicate mean ± SEM. GPR55 Het, *n*=3; GPR55 KO, *n*=3.

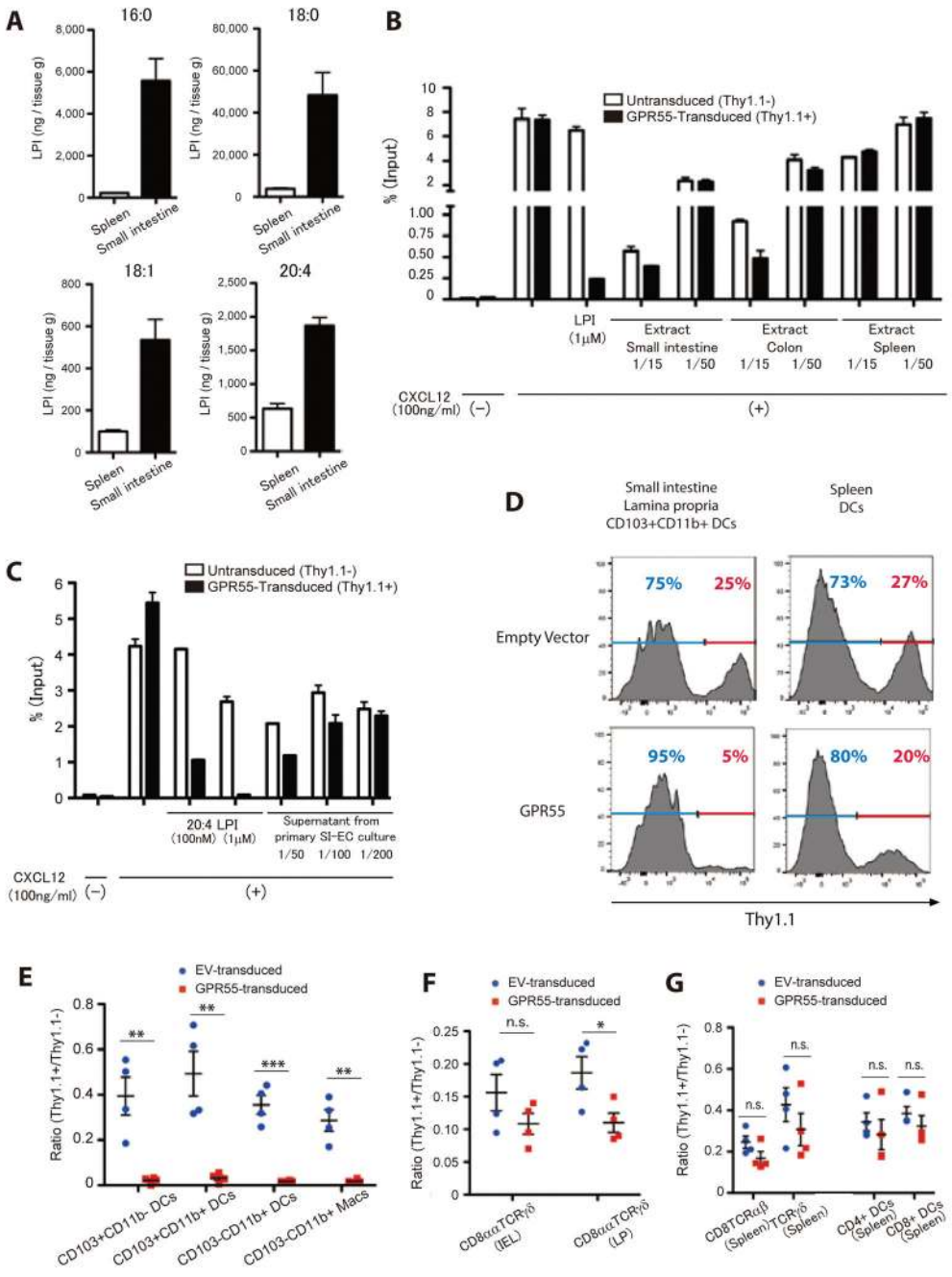

Fig. 3. Detection of GPR55 ligand in the small intestine

(**A**) Abundance of the indicated forms of LPI in spleen (*n*=5) and small intestine (*n*=5) tissue determined by LC-MS/MS. (**B**, **C**) Bioassay measurement of relative GPR55 ligand activity in small intestine, colon and spleen extract (**B**) and in small intestinal epithelial cell culture supernatants (**C**). WEHI231 cells transduced with GPR55 were tested for their response to the tissue extracts in a Transwell migration assay. Extract at the indicated dilution were mixed with CXCL12 (100ng/ml). Each experiment was performed in duplicate and repeated three times. (**D**) Histograms showing Thy1.1 reporter expression on intestinal and spleen DCs in mice that had been reconstituted with empty vector or GPR55 transduced BM. (**E–**

G) Summary data from mice of the type in d, shown as the ratio of Thy1.1+/Thy1.1− cells of the indicated types within the intestine (**E**, **F**) and spleen (**G**). n=4 in each group. ** p<0.01, * p<0.05, 'n.s.' p>0.05 by Student's t-test.

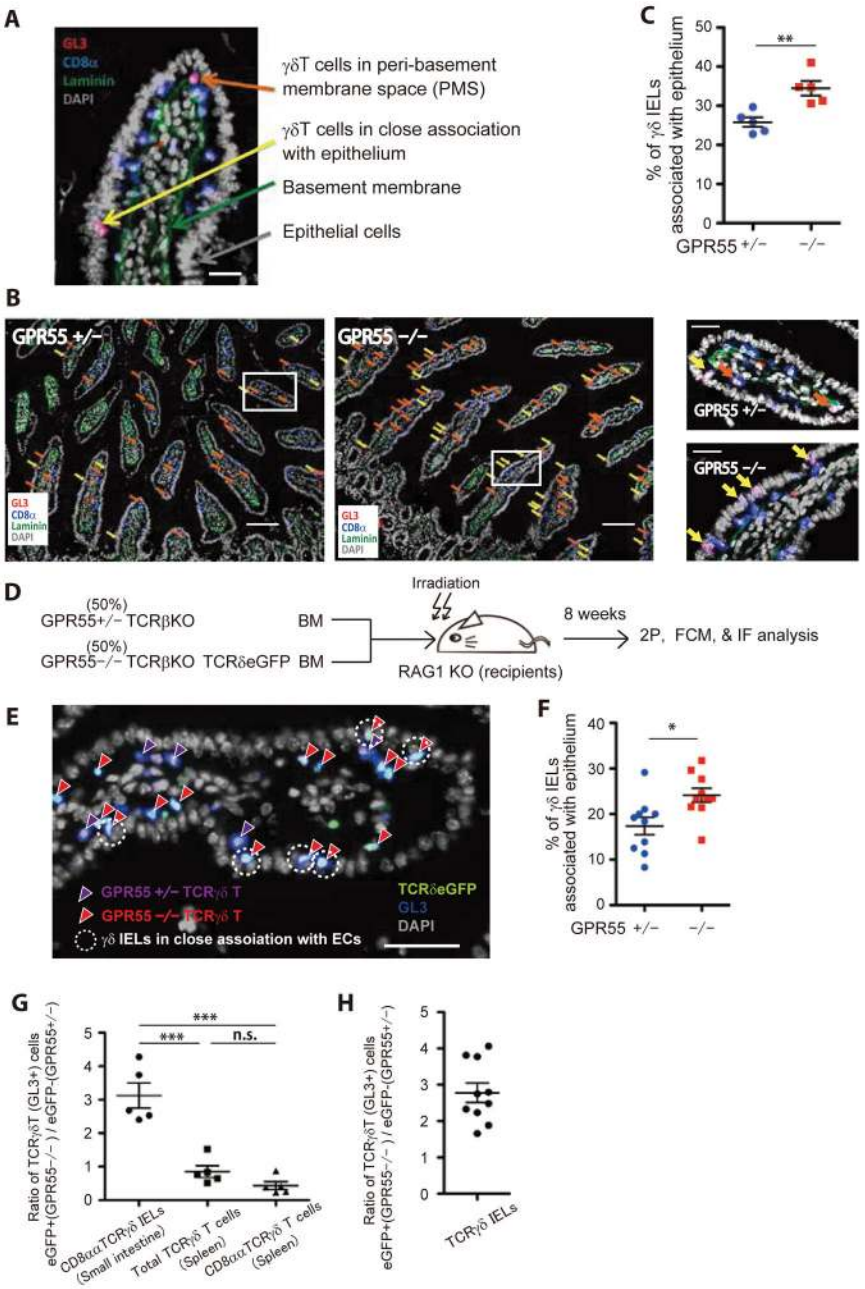

Fig. 4. Altered distribution of γδT IELs in GPR55-deficient mice

(**A**) Immunofluorescence detection of GL3 (γδTCR), CD8α, laminin and DAPI with examples of CD8α+GL3+ cells in the peri-basement membrane space (PMS) and in close association with the epithelium are highlighted. Scale bar, 20μm. (**B**) Distribution of CD8α+ γδT cells in the small intestine. In the left panels yellow arrows are used to highlight cells in close association with the epithelium and orange arrows cells associated with the PMS. Images are representative of 5 mice of each type. Scale bar, 100μm. Enlarged images from rectangles in left panels are shown on the right. Scale bar, 25μm. (**C**) Percentage of γδ IELs closely associated with epithelium in GPR55 Het and KO mice. (**D**) Diagram explaining the mixed BM chimera approach used to track control and KO γδT IELs in the same mice. (**E**)

Immunofluorescence analysis of control (Het, purple arrowheads) and GPR55 KO (red arrowheads) γδT IELs in the small intestine of a mixed BM chimeric mouse (n=10). Circles show regions where IELs are localized in close association with epithelial cells. Scale bar, 50μm. (**F**) Fraction of GPR55 Het and KO γδT IEL, identified as in E, located in close association with the epithelium. (**G**) Ratio of γδT cells of KO versus Het origin in the small intestinal IELs and spleen compartments determined by flow cytometry (n=5). (**H**) Ratio of γδT cells of KO versus Het origin in the small intestine determined by microscopy as in E (n=10). ***p<0.001, **p<0.01, *p<0.05, 'n.s.' p>0.05 by Student's t-test (**C**, **F**) or one-way ANOVA (**G**).

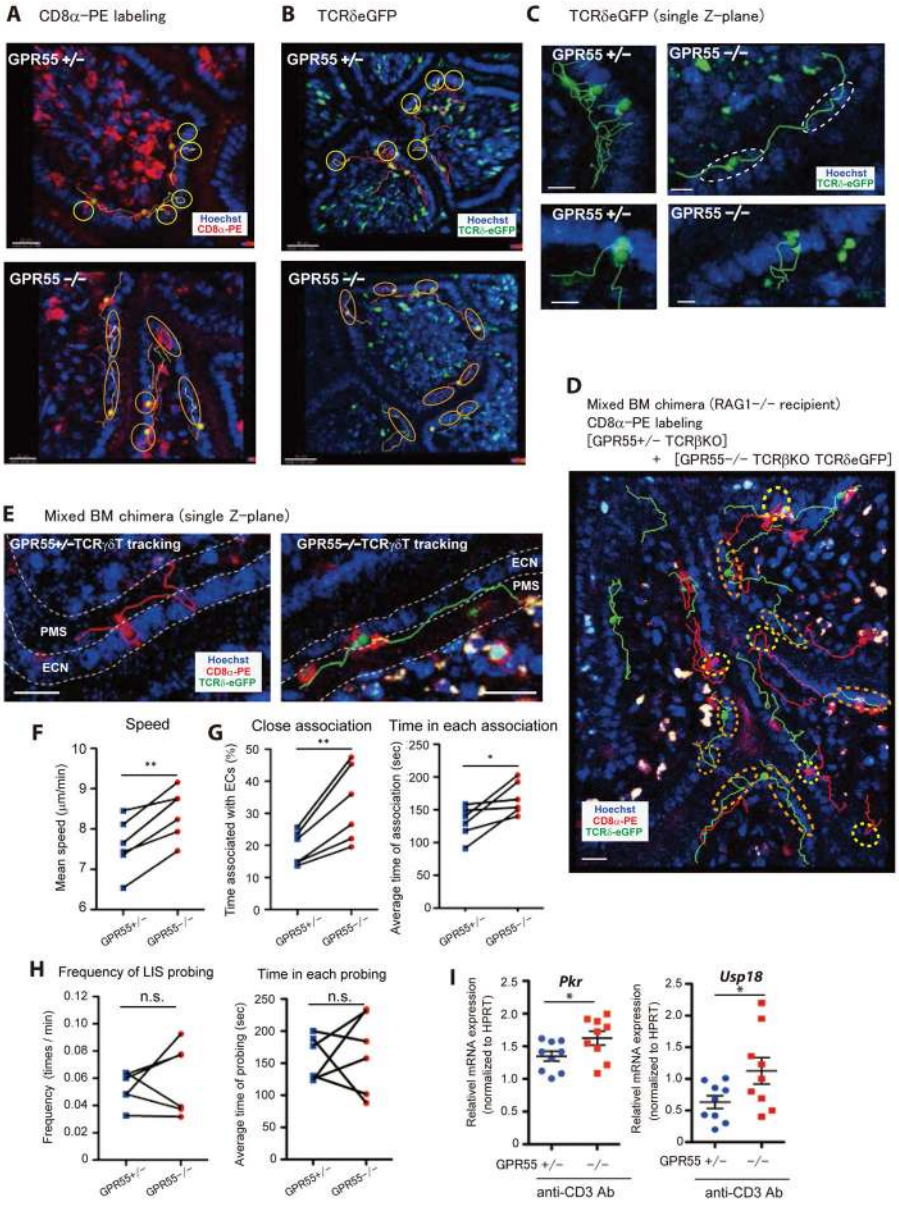

Fig. 5. Increased movement of GPR55 KO cells in association with epithelial cells

(**A**) Representative z-projection view of small intestinal villi of GPR55 Het (upper panel) and KO (lower panel) mice, showing CD8α-PE labeled cells (red) and cell nuclei (Hoechst, blue). Lines show tracks of labeled IELs. Images are representative from more than 6 mice in each genotype. Scale bars, 20μm. (**B**) Representative z-projection view of small intestinal villi of TCRδ–eGFP+ GPR55 Het (upper panel) and KO (lower panel) mice, showing eGFP (green) and cell nuclei (Hoechst, blue). Lines show tracks of GFP+ cells. Circles and ovals in A and B show regions of tracks that are localized in close association with epithelial cells. Images are representative from more than 7 mice in each genotype. Scale bars, 40μm. (**C**) Representative snap shots from single Z-plane movies. Left two panels from GPR55 Het and right two panels from GPR55 KO. Close association movement along epithelium observed as overlap of eGFP signal with the fluorescence signal of the epithelial cell nuclei labeled

with Hoechst (circles in right upper panel). Scale bars, 10μm. (**D**, **E**) Representative multiple Z-stack-projection view (**D**) and single Z-plane view (**E**) of small intestinal villi of mixed BM chimeras of the type described in Fig. 4D. Red cells are Het (red tracks) while red and green double positive cells are KO (green tracks). Ovals in D (yellow in Het and orange in KO) show regions of tracks that are localized in close association with epithelial cells. Dashed white lines in E indicate the boundaries of the Hoechst labeled epithelial cell nuclei (ECN) and the peri-basement membrane space (PMS) used for the quantitation. Images are representative from 6 mice. Scale bars, 20μm. (**F**) Speed of GPR55 Het and KO γδT IELs in mixed BM chimeras. (**G, H**) Percentage of time in close association with epithelial cells and time of each association (**G**), and frequency of lateral intercellular space (LIS)-probing, and time of each probing (**H**) of GPR55 Het and KO cells in mixed BM chimeras. Combined data from 6 movies from 6 different chimeric mice. (**I**) Induction of *Pkr* and *Usp18* mRNA in the small intestine of GPR55 Het and KO mice treated with anti-CD3 Ab for 3 hours, plotted relative to *Hprt*. Combined data from two independent experiments (n=9 in each group).***p<0.001, **p<0.01, * p<0.05, 'n.s.' p>0.05 by Student's t-test.

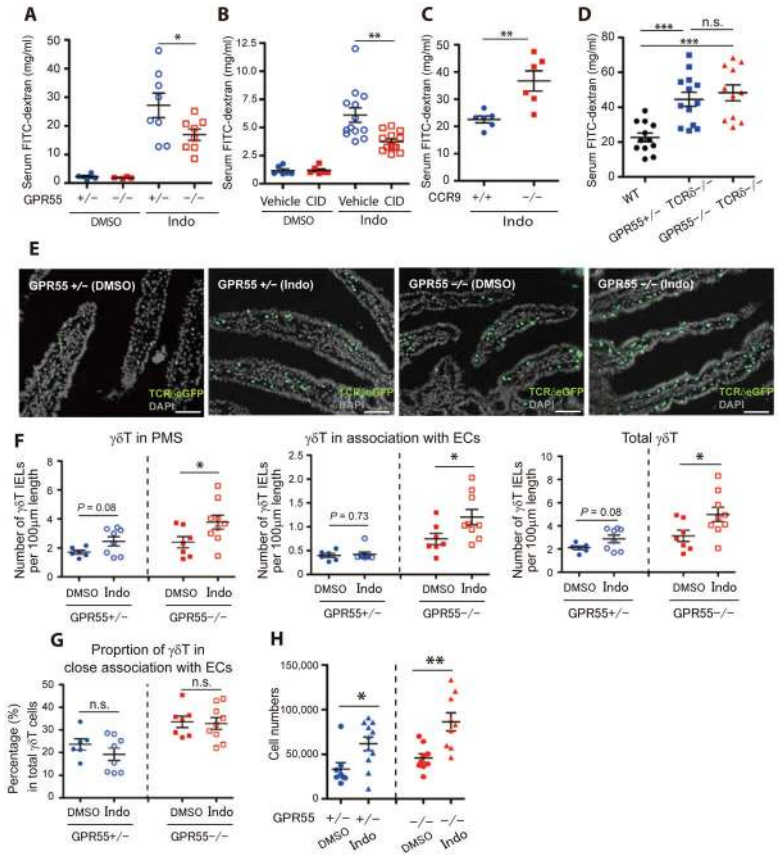

Fig. 6. Increased resistance of GPR55-deficient mice to indomethacin induced intestinal permeability

(**A–D**) Serum FITC-dextran in GPR55 Het (DMSO, *n*=4; Indo, *n*=8) and KO (DMSO, *n*=4; Indo, *n*=8) mice (**A**), WT mice treated with vehicle (DMSO, *n*=6; Indo, *n*=13) or GPR55 antagonist CID16020046 (DMSO, *n*=6; Indo, *n*=13) (**B**), CCR9 WT (*n*=6) and KO (*n*=6) mice (**C**) or in WT (*n*=12), GPR55 Het TCRδ KO (*n*=13) and GPR55 KO TCRδ KO (*n*=11) mice (**D**), all treated for 5 hours with vehicle (DMSO) or indomethacin (Indo) and for 4 hours with FITC-dextran. (**E**) Immunofluorescence detection of TCRδ–eGFP and DAPI in GPR55 Het and KO mice treated with carrier (DMSO) or indomethacin (Indo) for 4 hours. Scale bars, 50μm. (**F**) Number of γδT IELs (number per 100um length) beneath (in PMS) or closely associated with the epithelium, or in both compartments of GPR55 Het (DMSO, *n*=6; Indo, *n*=7) or KO (DMSO, *n*=8; Indo, *n*=9) mice treated with DMSO on Indo as in E. (**G**) Percentage of γδT IEL in close association with the epithelium. (**H**) Number of γδT IEL in GPR55 Het (DMSO, *n*=7; Indo, *n*=11) and KO (DMSO, *n*=9; Indo, *n*=9) mice 4 hours after DMSO or Indo treatment as determined by flow cytometry. ***p<0.001, **p<0.01, * p<0.05, 'n.s.' p>0.05 by Student's *t*-test (A, B, C, F, G, H) or one-way ANOVA (D).

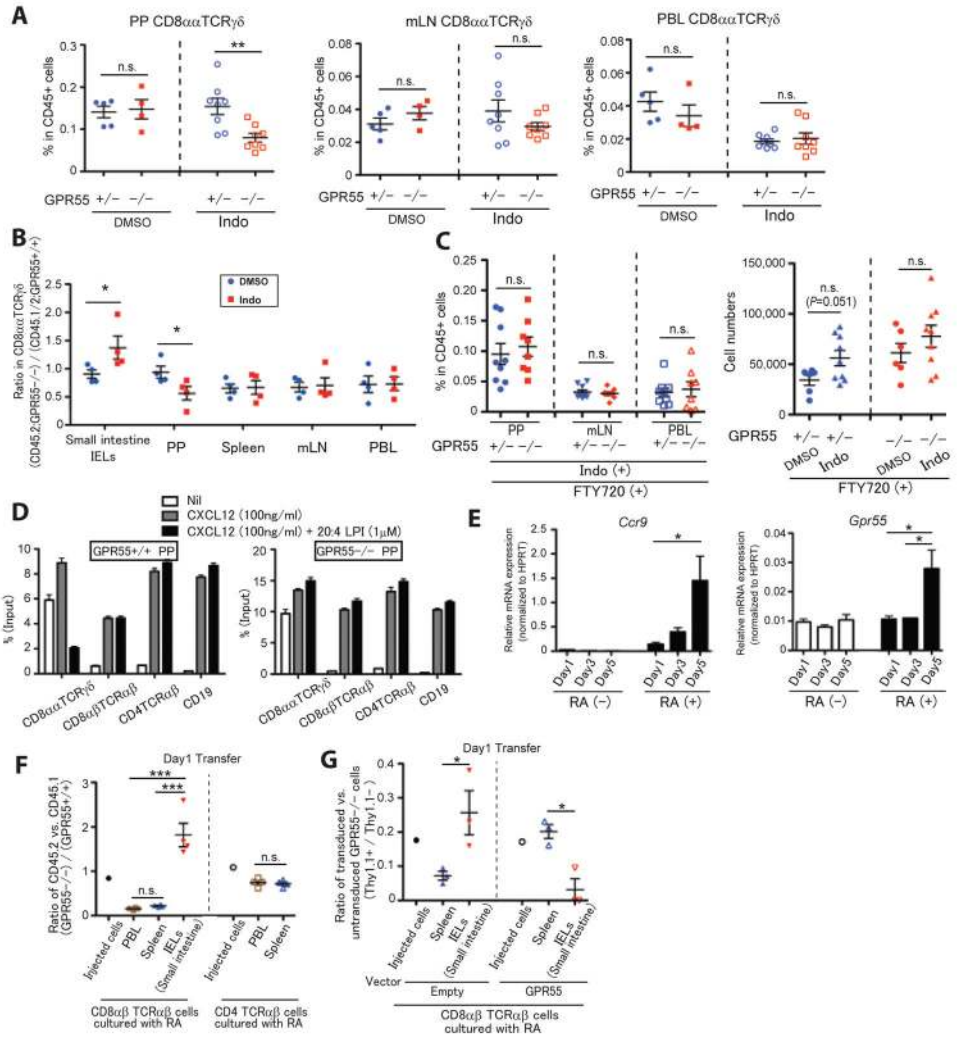

Fig. 7. GPR55 regulates γδT cell egress from Peyer's patches and homing of gut tropic CD8 T cells to the small intestine

(**A**) Frequency of CD8αα γδT cells in Peyer's patches (PP), mesenteric lymph node (mLN) and peripheral blood lymphocyte (PBL) of GPR55 Het (DMSO, *n*=5; Indo, *n*=8) and KO (DMSO, *n*=4; Indo, *n*=8) mice after treatment with carrier (DMSO) or indomethacin (Indo) for 4 hours. (**B**) Ratio of CD45.2 GPR55 KO over CD45.1/2 GPR55 WT CD8αα γδT cells in the indicated tissues of mixed BM chimeras, 4 hours after treatment with DMSO or Indo (*n*=4 in each group). (**C**) Percentage (left panel) or numbers (right panel) of CD8αα γδT cells in the indicated GPR55 Het and KO mouse tissues after treatment for 4 hours with Indo and FTY720. Left panel: GPR55 Het, *n*=9; GPR55 KO, *n*=8. Right panel: GPR55 Het, *n*=6; GPR55 KO, *n*=9. (**D**) Migration of the indicated cell types from PPs of control and GPR55 KO mice to nil, CXCL12 or CXCL12 and 20:4 LPI in Transwell assays. Each experiment was performed in duplicate and repeated twice. (**E**) Expression of *Ccr9* and *Gpr55* mRNA on T cells cultured for the indicated days in the presence of anti-CD3, anti-CD28 and with 100U/ml IL-2 from day 3, and in the absence or presence of retinoic acid (RA), plotted relative to *Hprt* (*n*=4 in each group from two independent experiments). Bars indicate mean

± SEM. (**F**) Homing of CD8 T cell cultured with RA as in E to spleen, small intestine and blood, shown as the ratio of CD45.2 GPR55 KO cells to CD45.1 WT cells, 1 day after transfer. Data (n=4 in each group) are representative of two independent experiments. (**G**) Homing of cells cultured as in E and transduced with empty or GPR55-containing vector, plotted as the ratio of transduced (Thy1.1 reporter positive) to untransduced (Thy1.1 reporter negative) cells of each type, 1 day after transfer. 'Injected cells' in F and G indicates the ratio at the time of injection. Data (n=3 in each group) are representative of two independent experiments. ***p<0.001, **p<0.01, *p<0.05, 'n.s.' p>0.05 by Student's t-test (A, B, C, F, G) or one-way ANOVA (E).